ELSEVIER

Astroparticle Physics 12 (1999) 121–134

Astroparticle Physics

www.elsevier.nl/locate/astropart

Geometrical reconstruction with the High Resolution Fly's Eye prototype cosmic ray detector

C.R. Wilkinson[a,1,2], T. Abu-Zayyad[b], M. Al-Seady[b], K. Belov[b], D.J. Bird[a,2], J. Boyer[c], G. Chen[b], R.W. Clay[a], H.Y. Dai[b,3], B.R. Dawson[a], Y. Ho[c], M.A. Huang[b,4], C.C.H. Jui[b], M.J. Kidd[d,3], D.B. Kieda[b], B.C. Knapp[c], W. Lee[c], E.C. Loh[b], E.J. Mannel[c], J.N. Matthews[b], T.A. O'Halloran[d], A. Salman[b], K.M. Simpson[a], J.D. Smith[b], P. Sokolsky[b], P. Sommers[b], S.B. Thomas[b], L.R. Wiencke[b], N.R. Wild[a]

[a] *Dept. of Physics and Mathematical Physics, The University of Adelaide, S.A., 5005, Australia*
[b] *Department of Physics and the High Energy Astrophysics Institute, University of Utah, UT, 84112, USA*
[c] *Columbia University, Nevis Laboratories, Irvington, NY, 10533, USA*
[d] *Department of Physics, University of Illinois at Urbana-Champaign, IL, 61801, USA*

Received 31 January 1999; accepted 18 May 1999

Abstract

The High Resolution Fly's Eye EHE cosmic ray detector (HiRes) was operated for over two years (prior to November 1996) in a two-site prototype configuration. This paper describes the development and testing of an event reconstruction method for extensive air showers (EAS) viewed in coincidence by both sites (stereo viewing). The reconstruction accuracy was directly measured through the use of a UV laser mounted on a telescope that generated airshower-like events with known geometries. For events observed with stereo opening angles greater than about 10° (most events) the median error in the reconstructed laser direction was 0.4° with 95% of events being reconstructed with errors of less than 0.9° (which degrade to 0.8° and 1.8°, respectively, for smaller opening angles). A limited investigation of the likely performance of the HiRes Stage 1.0 detector was undertaken. Reconstruction accuracy is likely to be only slightly degraded compared with the prototype results.

1. Introduction

The High Resolution Fly's Eye (HiRes) is a second generation atmospheric fluorescence detector for extremely high energy (EHE) cosmic rays ($E > 10^{18}$ eV) [1]. It builds upon the experience gained with the

[1] Corresponding author; Defence Science Technology Organisation, PO Box 1500, Salisbury, SA 5108, Australia; E-mail: Christopher.Wilkinson@dsto.defence.gov.au.
[2] Now at Defence Science Technology Organisation, PO Box 1500, Salisbury, SA 5108, Australia.
[3] Now at Rosetta Inpharmatics, 12040 115th Ave NE, Kirkland WA 98034, USA.
[4] Now at Institute of Physics, Academia Sinica, 11529 Nankong, Taiwan, R.O.C.

0927-6505/99/$ - see front matter
PII S0927-6505(99)00087-0

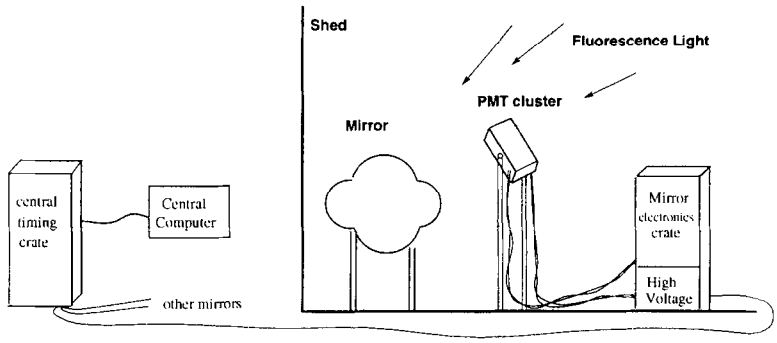

Fig. 1. The basic HiRes data acquisition system.

Fly's Eye detector [2] and has been designed with the specific goals of (a) increasing the data rate above 10^{19} eV to > 200 events per year; (b) improving the depth of shower maximum (X_{max}) resolution to less than 20 g cm^{-2}; and (c) improving the angular resolution and acceptance of the detector so as to increase sensitivity to point sources. These goals will be achieved through the construction of a two-site detector utilising improved optics, electronics, and analysis techniques [3]. The purpose of this paper is to describe the analysis techniques developed for reconstruction of stereo observations of EAS. Tests performed with the prototype detectors will also be discussed.

In this paper we will begin with an overview of the HiRes detector before describing the reconstruction analysis techniques. This will be followed by a discussion of the testing of the reconstruction programs and the results of the testing process. Finally, the likely reconstruction accuracy for the HiRes Stage 1.0 detector is briefly investigated.

2. The High Resolution Fly's Eye cosmic ray detector (HiRes)

The High Resolution Fly's Eye cosmic ray detector [4,5] is an optical detector designed to measure the isotropic nitrogen fluorescence light generated by the passage of a cosmic ray induced EAS through the atmosphere. The detector is located at Dugway Proving Grounds in Utah, USA, and consists of two sites separated by 12.6 km. Each site houses a number of mirror units. Each mirror unit consists of a fixed 4.2 m^2 spherical mirror which focuses light onto an array of 256 photomultiplier tubes (PMT) located behind a UV bandpass (300–400 nm) filter. Each PMT within the array has a fixed field of view of approximately 1°. The mirrors are arranged to form a composite eye (analogous to a fly's eye) which passively views a section of sky for fluorescence signals produced by EAS. Due to the weak nature of this signal and the desire to maximise the aperture, operation is limited to dark sky (moonless) conditions. An overview of the system is presented in Fig. 1.

Global Positioning System-based clocks are used at each site to ensure relative time synchronisation to within 50 ns (and absolute time to within 340 ns of UTC) [6,1]. PMT trigger thresholds are dynamically adjusted to maintain a constant trigger rate and PMT trigger times, within mirrors, are recorded to nanosecond accuracy. PMT signals are passed through two integration (sample-and-hold) channels (after a delay to allow trigger formation), with one channel optimised for nearby showers (short integration time) and the other for more distant showers. Intermirror trigger times are recorded to 25 ns accuracy [7,8,1].

The HiRes-2 site is located 12.6 km to the south-west of the HiRes-1 site [9] and the two eyes have overlapping fields of view towards the northeast of HiRes-1 as indicated in Fig. 2. The prototype configuration consisted of 14 mirrors at the HiRes-1 site (in 5 elevation "rings" covering 3°–70°) and 4 mirrors at the HiRes-2 site (in 2 elevation "rings" covering 3°–30°). The two site prototype detector ran for almost two years

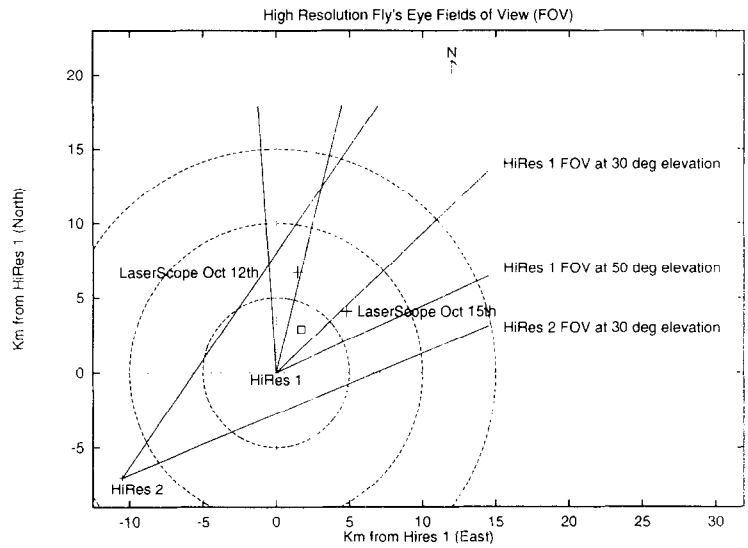

Fig. 2. A plan view of the location of HiRes-1 and HiRes-2 at Dugway Proving Ground and their fields of view. The dashed circles represent distances of 5, 10 and 15 km from HiRes 1, the crosses indicate the positions of the Laserscope used for testing the reconstruction programs, and the square denotes the sire of the CASA/MIA arrays.

before being shut down in November 1996 to make way for construction of the Stage 1.0 detector.

The stage 1.0 detector consists of 22 mirrors at HiRes-1 forming a full azimuthal ring of mirrors covering elevation angles from 3°–17°, and 42 mirrors at HiRes-2 comprising of two stacked full azimuthal rings that cover elevation angles from 3°–30° [10]. HiRes-1 mirrors will utilise the sample-and-hold electronics of the prototype, whilst HiRes-2 mirrors will be instrumented with newly developed Flash ADC (FADC) electronics [11,12].

3. Reconstructing trajectories for stereo viewed Extensive Air Showers (EAS)

An extensive air shower moves through the atmosphere at the speed of light, isotropically emitting fluorescence light as it develops along an axis that points back to the arrival direction of the primary particle (Fig. 3). Correct determination of the trajectory is vital for analysing all information from an event. It goes far beyond simply determining the cosmic ray arrival direction. A precise trajectory is the first step towards an accurate reconstruction of the longitudinal shower development profile and the primary cosmic ray energy. This is due to the fact that one has to take into account the propagation and attenuation of light from the shower to the detector.

Determination of the EAS trajectory is, in principle, straightforward. At each site viewing the EAS, a series of triggered PMTs will define a great circle on the celestial sphere. One can then define the Shower-Detector Plane (SDP) as the plane containing this great circle and the detector, as shown in Fig. 3. The shower trajectory can now be found using information from either one, or two sites (mono and stereo reconstruction, respectively). Mono reconstruction utilises PMT triggering times to determine the orientation of the shower within the SDP (illustrated in Fig. 4) whilst stereo reconstruction uses the intersection of SDP's from two sites to obtain the shower trajectory (illustrated in Fig. 5). If sites are well synchronised and timing systematics are accounted for, PMT trigger time information from two sites may be combined to reconstruct the EAS trajectory (known as "timing" reconstruction). In practice, complications arise due to effects such as triggers on sky noise, atmospheric scattering, finite shower width, trigger time slewing, and optical aberrations. There is, however,

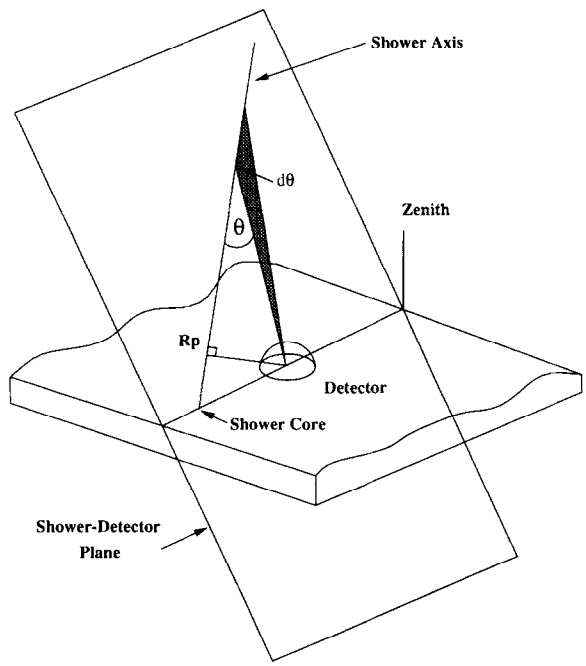

Fig. 3. Geometry of an EAS illustrating the Shower-Detector Plane (SDP) for a single site. Light is emitted from the EAS and is viewed by a PMT with a light emission angle theta. Each PMT has a 1° fixed field of view hence views only a section of the EAS denoted by $d\theta$. A succession of PMTs will view the EAS, and their pointing directions combined with their light intensity information can be used to determine the SDP.

obvious scope for combining elements from stereo and timing techniques.

Experience with the Fly's Eye detector indicated that stereo reconstruction (using only geometrical information from the two eyes) was superior to mono reconstruction (using geometrical and timing information from one eye), except in the small opening angle case. When the opening angle, α, between the two SDP's approaches zero, stereo reconstruction breaks down. Monte Carlo simulations of the Stage 1.0 HiRes detector have indicated that the best reconstruction accuracy should be achieved with techniques utilising both geometrical and timing information from the two sites (stereo-timing fitting) [13].

A combined stereo-timing fitter was developed for the prototype detector. The approach taken was to develop a composite χ^2 function and use the downhill simplex method [14] to find the true trajectory. This required searching over five dimensions – four to define the trajectory (zenith angle, azimuth angle, and the (East, North) core location in the plane tangent to the surface of the earth at HiRes-1) and one for the clock synchronisation offset between the two sites. The downhill simplex method begins by selecting a trial trajectory and a synchronisation offset. A χ^2 value is then determined using a function which compares the measured light amplitudes and trigger times for the firing PMTs with those expected for the trial geometry. To ensure success, one aims to use a χ^2 function which closely approximates the true detector response.

The composite stereo-timing χ^2 is a function given by

$$\chi^2_{\text{Total}} = \chi^2_{1\ \text{Stereo}} + \chi^2_{2\ \text{Stereo}} + \chi^2_{1\ \text{Time}} + \chi^2_{2\ \text{Time}} + \chi^2_{1-2\ \text{Offset}}. \tag{1}$$

The $\chi^2_{1\ \text{Stereo}}$ and $\chi^2_{2\ \text{Stereo}}$ terms represent the stereo contributions to the fit from the two sites. The $\chi^2_{1\ \text{Time}}$ and $\chi^2_{2\ \text{Time}}$ terms are the time fit components from the two sites and the $\chi^2_{1-2\ \text{Offset}}$ term represents the fit to the time synchronisation offset between the two sites. Stereo fitting utilises only the first two terms, whilst time fitting utilises only the last three.

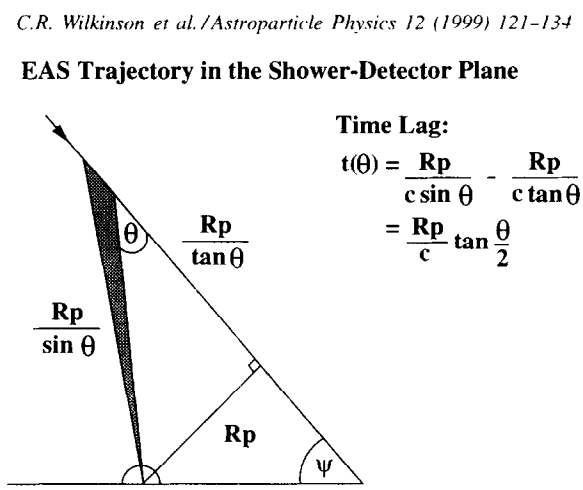

Fig. 4. The mono method for estimating the shower trajectory. Determining the time lag for a PMT viewing an emission angle of θ within the SDP. The origin of time is assumed to be the time at which a planar shower front (of infinite extent) passes through a point representing the detector. The equation returns the arrival time of light at a PMT. The shaded region represents the field of view of the PMT, which needs to be taken into account if the track segment is relatively bright (or dim) as this causes the PMT to trigger earlier (later) than expected (since the effective emission angle differs from the nominal value given by the PMT's pointing direction). The orientation of the trajectory within the SDP is defined by the impact parameter R_p, and the angle, Ψ, between the trajectory and the ground.

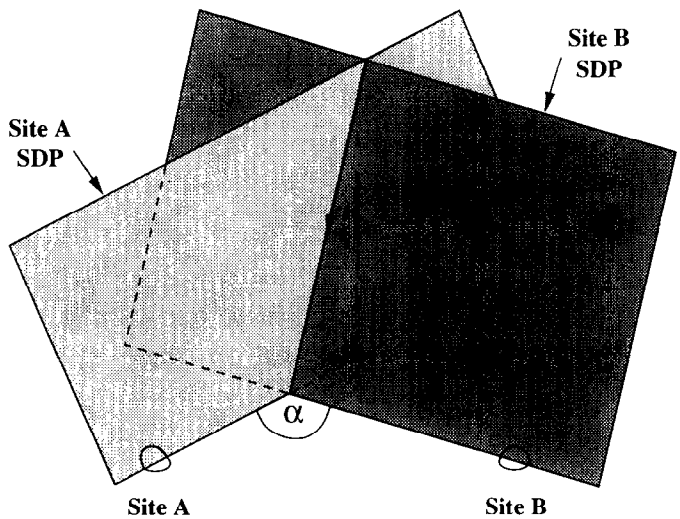

Fig. 5. The stereo method for estimating the shower trajectory. The shower is viewed by two sites each of which determine a shower–detector plane. The EAS trajectory is then the intersection of these two SDP's. The stereo opening angle, α (indicated) is actually the angle between the normal vectors of the two SDPs.

Several functional forms for the stereo χ^2 component were investigated with the best results obtained using an amplitude weighted form given by

$$\chi_i^2 = \omega_i \frac{(\mathrm{PMT_i\ amplitude} - \mathrm{Expected\ Amplitude})^2}{\sigma^2};$$

$$\text{where } \omega_i = \frac{\mathrm{PMT_i\ Amplitude}}{\mathrm{Average\ PMT\ Amplitude}},$$

$$\text{Expected Amplitude} = \text{Ray Tracing Response} \times \text{Average Flux at PMT}_i\,.$$

and $\sigma^2 = \text{PMT}_i \text{ Amplitude} + \text{Sky Noise} + 0.05 \times \text{Expected Amp}.$ (2)

Here ω_i represents the amplitude weighting term. Amplitude weighting is a simplistic fitting method which works on the assumption that PMTs will trigger provided the EAS passes through their field of view, and that those PMTs with the largest amplitudes are those most directly viewing the central axis of the EAS. Amplitude weighting seeks to prevent the fitter from being biased due to the effects of atmospheric scattering (which may be non-uniform about the track), noise PMTs (which are weak but randomly placed), and low light intensities at the start or end of an EAS.

The numerator in Eq. (2) is the χ^2 function for comparing measured and expected light amplitudes for a trial SDP. The expected amplitude takes into account the way the light spot crosses the PMT (e.g. a track through the tube center or a track just clipping the edge) and the angular offset of the PMT from the EAS track (the PMT's "off plane" angle). Ray tracing calculations and empirical measurements of the PMT photocathode response have been performed and combined to produce the estimated response of a PMT to a constant light flux for a given trial plane. These estimated responses are then scaled to the actual light flux over the mirror when a given PMT is triggered. This flux is estimated by averaging the flux from all PMTs within 3° of the PMT in question on the assumption that the flux should change smoothly along the track.

The σ^2 error term in Eq. (2) takes into account Poisson fluctuations in the measured PMT amplitude, the effect of sky noise during the PMT integration, and an arbitrary 5% error in the estimated amplitude. This last term is due to uncertainty in the estimated flux and errors in the calculated PMT response. Recent work with the Laserscope (described below) in measuring the response profile of PMTs [15] has indicated some deficiencies in the PMT response parameterisation used. Further work is underway to improve the PMT response profile estimates. However, for the present analysis, the original response profile results have been used together with the above 5% error term.

To derive the timing χ^2 components we turn to Fig. 4 which illustrates the orientation of an EAS within a SDP. A PMT which views the EAS at an angle θ_i triggers at a time $t(\theta_i)$ with respect to the time at which the shower front would pass through the detector (assuming, as above, it was both flat and infinite in extent). This time lag is given by $(R_p/c)\tan(\theta_i/2)$ (noting that the values for R_p and θ_i will depend on the geometry of the trial trajectory). Another fitted parameter is a timing offset, t_{offset}. The measured times are referenced to the time of the first PMT trigger, t_0. Hence, a timing χ^2 function can be constructed by comparing the expected triggering times (which will depend on the trial trajectory) with the actual triggering times,

$$\chi_i^2 = \frac{\{[(R_p/c)\tan(\theta_i/2) - t_{\text{offset}}] - (t_i - t_0)\}^2}{\sigma_{t_i}^2}. \tag{3}$$

This technique relies upon a good knowledge of PMT triggering times. As indicated by Fig. 4, each PMT actually views an extended section of the EAS trajectory. To correctly estimate the triggering time of a PMT, one must determine the emission angle, θ, of light from the EAS at the time of triggering. This is equivalent to estimating what fraction of the light spot has crossed the tube aperture at the time of triggering. To a first approximation the emission angle can be set to the angle between the trial shower axis and the pointing direction of the PMT center. However, since a tube trigger is based on its current exceeding a pre-set threshold, bright tracks will trigger the PMT soon after the light spot starts crossing the PMT, whilst dim tracks may trigger significantly later, an effect known as time-slewing. To properly compensate for this systematic effect, one must know the pulse shape in the PMT. This is partly determined by the energy (amplitude) and distance (crossing time) of the EAS. Pulse shape information was unavailable with the sample-and-hold electronics used by the prototype detectors, but will be available with the new FADC electronics of the Stage 1.0 detector. Attempts have been made to compensate for the effects of time slewing, but the difficulties and uncertainties eventually limit the usefulness of time fitting with sample-and-hold electronics [1].

It should be noted that time fitting is problematic for EAS with small observed angular track lengths. In such cases the $\tan(\theta/2)$ function is approximately linear over the small angular range of measurements and errors

in fitting for R_p and Ψ become correlated (see Kidd [16] for details). For time fitting to be effective, the data are required to exhibit curvature in $(\theta, (t_i - t_0))$ space. Note that σ_t represents the uncertainty in the triggering time of the PMT. Whilst, within a mirror, relative PMT triggering times are precise to several nanoseconds, mirrors are only synchronised to within 25 ns, somewhat increasing the trigger time uncertainty.

Finally, the last component in Eq. (1) describes the synchronisation offset between the clocks at the two sites. It has the form

$$\chi^2_{1-2\ \mathrm{Offset}} = \frac{(\mathrm{HiRes\ 1} - \mathrm{HiRes\ 2\ Clock\ Offset})^2}{\sigma_{1-2\ \mathrm{Offset}}}. \tag{4}$$

where $\sigma_{1-2\ \mathrm{Offset}}$ is an estimate of the synchronisation uncertainty.

4. Reconstruction accuracy

A telescope-mounted UV laser known as the Laserscope [15] was used to produce a set of laser shots with known geometries for testing the reconstruction accuracy. The laser fires a collimated beam into the atmosphere from which light is scattered towards the detector producing a track very similar to an EAS track. The two main differences between EAS and laser shots are that laser shots are upward going instead of downward going and the shower development profile is different from that of a cosmic ray induced EAS. The advantage of the system is that it is capable of producing a large data set of events with accurately known geometries. These events can be reconstructed, and the space angle between the actual and reconstructed trajectory can be determined. The distribution of space angles thus provides a direct estimate of the reconstruction accuracy of the fitting process.

The data used to check the accuracy of the reconstruction program were taken on the 12th and 15th of October 1996 and covered a wide range of geometries. A total of 4343 acceptable events covering stereo opening angles from 7° to 35° were taken on the 12th, and 6811 events covering stereo opening angles from 2° to 11° were taken on the 15th. Due to problems with the initial design of the Laserscope mount, the pointing accuracy of the Laserscope was 0.1°–0.3° for the 12th and 0.1°–0.5° for the 15th. These errors arose because the laser was not mounted rigidly enough, leading to a decrease in pointing accuracy as the telescope approached the zenith (the 0.1° was the measured error when the telescope was pointing horizontally). This effect was larger on the 15th due to a heavier Nitrogen laser being used in place of a YAG laser. Unfortunately this problem was only detected (and fixed) after data were taken. A sample Laserscope event and its reconstructed trajectory is presented in Fig. 6.

Space angle integral error distributions for the different reconstruction techniques applied to data from the 12th and 15th of October are presented in Figs. 7 and 8 and summarised in Tables 1 and 2, respectively. The errors in core location (in this case the Laserscope position) for data from the 12th are also presented in Table 3. Distributions of the component χ^2's and the total χ^2's (Eq. (1)) were also obtained with results for the total χ^2 per degree of freedom summarised in Tables 1 and 2. Well reconstructed events had small χ^2's and approximately balanced components. These reduced χ^2's were generally larger than 1, indicating that the expectation functions used were not perfect. Poorly reconstructed events generally had large χ^2's, allowing quality cuts to be made on the data by rejecting events with large χ^2 values. Requiring that the χ^2 per degree of freedom be less than 50 on stereo-timing data was found to suppress the tail in the space angle distribution as seen in Figs. 7 and 8 and Tables 1 and 2. Such a cut reduced the number of reconstructable events from 4343 to 4110 on the 12th and 6811 to 5743 on the 15th.

Stereo fitting performed well for large opening angles, with the accuracy degrading as the opening angle decreased. This opening angle effect is clearly visible when comparing space angle distributions from the two nights. Reconstruction of data taken on the 12th has a much tighter space angle distribution than data taken on

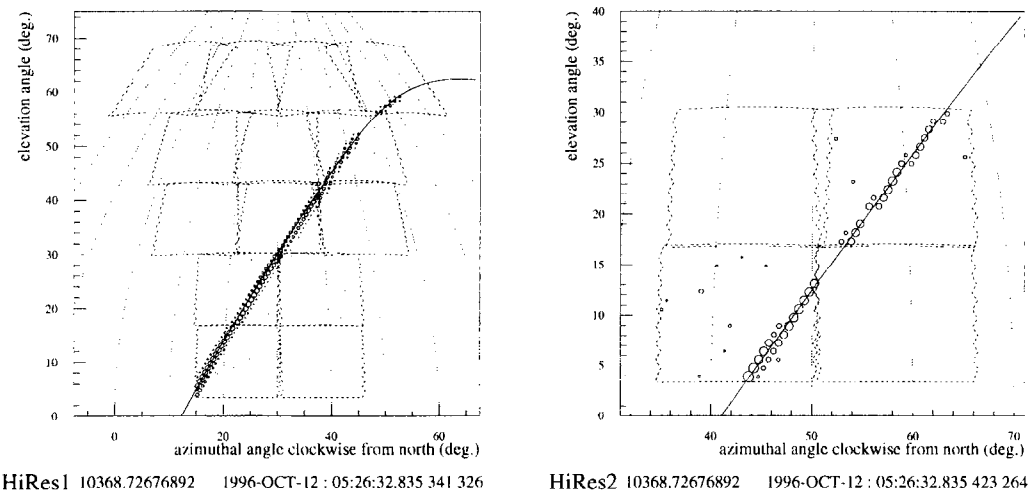

Fig. 6. An example of a Laserscope event showing the reconstructed shower-detector planes (indicated by lines on the the representation of the celestial sphere). Circles represent PMT signals, with larger circles denoting larger signals. This event was reconstructed with a space angle error of 0.42°. The space angle error is marginally worse at 0.43° if the event is reconstructed using the Stage 1.0 configuration (where we use only mirrors in the lowest elevation ring at HiRes-1).

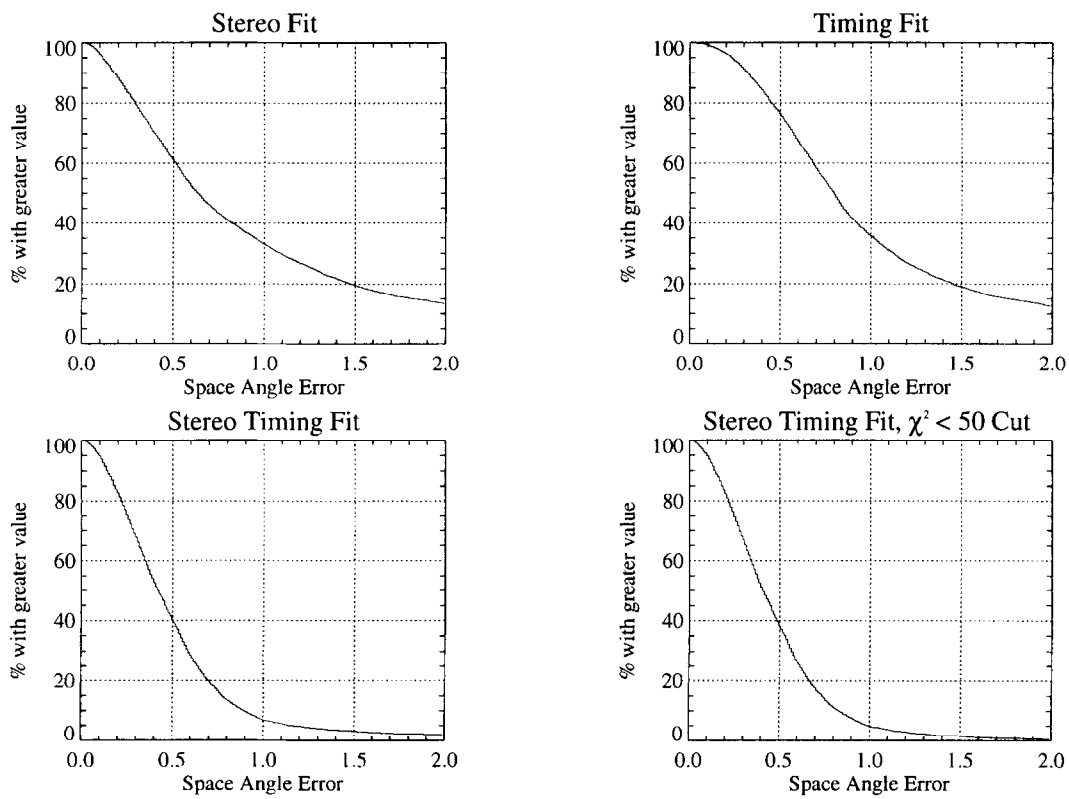

Fig. 7. Space angle integral error distributions (in degrees) for different fitting techniques based on the nominal directions of the Laserscope for data taken on the 12th of October 1996. Note how stereo performs slightly better than timing, and how reconstruction accuracy improves significantly when they are combined in stereo-timing fitting.

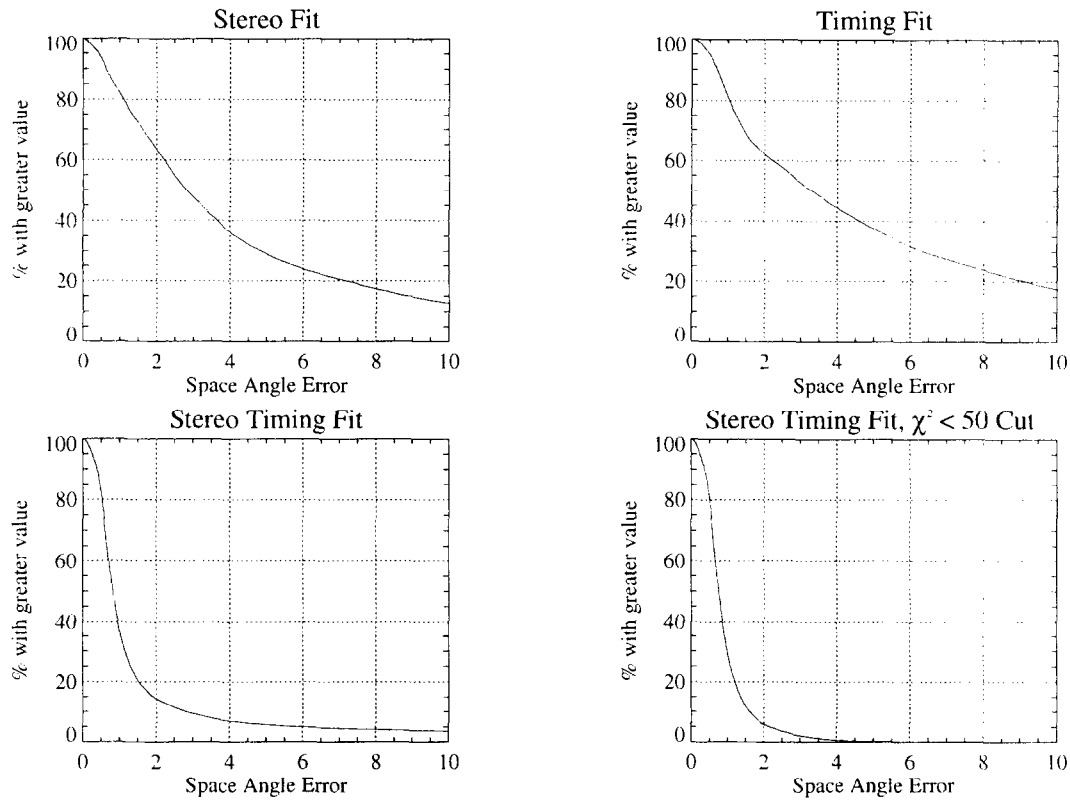

Fig. 8. Space angle integral error distributions for different fitting techniques based on the nominal directions of the Laserscope for data taken on the 15th of October 1996 (predominantly small opening angles). Note how stereo-timing fitting once again improves on either stereo or timing fitting (and that for these smaller opening angles stereo and timing perform approximately equally). Also note how application of a $\chi^2 < 50$ cut suppresses the tail of the distribution.

Table 1
Reconstruction results for stereo viewed laser shots taken on the 12th of October 1997

Fit type	Space angle			Fit χ^2 value	
	50%	90%	% > 2°	Median	FWHM
Stereo	0.65°	2.5°	13%	6	7
Timing	0.8°	2.3°	12%	8	8
Stereo-timing	0.4°	0.9°	1.7%	14	10
Stereo-timing $\chi^2 < 50$	0.4°	0.85°	0.7%	14	10

The space angle is the angle between the fitted and actual trajectories. Integral error distributions were obtained and the values containing 50% and 90% of the data are presented. Note how stereo performs better than timing, and that by combining the two in stereo-timing greatly increases the reconstruction accuracy. All quoted χ^2 values are per degree of freedom. Placing a cut of $\chi^2 < 50$ enabled rejection of poorly reconstructed events (5% of the total number of events).

the 15th which have much smaller opening angles. Apart from any opening angle effects, the distribution from the 15th is expected to be slightly worse than that from the 12th due to problems with the Laserscope mount.

Time fitting was also investigated, and found to be slightly worse than stereo in most cases. Whilst time fitting was not subject to opening angle effects present in stereo fitting, uncertainty in the PMT triggering times meant that time fitting did not perform better than stereo in the case of small opening angles. It is interesting to note

Table 2
Reconstruction results for stereo viewed laser shots taken on the 15th of October 1996

Fit type	Space angle			Fit χ^2 value	
	50%	90%	% > 10°	Median	FWHM
Stereo	2.75°	11.5°	13%	10	12
Timing	3.3°	14.7°	17%	8	7
Stereo-timing	0.9°	2.9°	3%	19	12
Stereo-timing $\chi^2 < 50$	0.8°	1.8°	0.05%	19	12

Note the poor resolution with either stereo or timing reconstruction due to small opening angles, and how stereo-timing improves the reconstruction accuracy. Placing a cut of $\chi^2 < 50$ enabled rejection of poorly reconstructed events (16% of the total number of events).

Table 3
Reconstruction results for stereo viewed laser shots taken on the 12th of October 1996

Fit type	$\langle X \text{ core} \rangle \pm 1\sigma$ (km)	$\langle Y \text{ core} \rangle \pm 1\sigma$ (km)	R core error	
			50%	% > 0.25
True position	1.459	6.708	(km)	(km)
Stereo	1.451 ± 0.06	6.659 ± 0.11	0.065	9%
Stereo-timing	1.452 ± 0.04	6.682 ± 0.08	0.050	3%
Stereo-timing $\chi^2 < 50$	1.452 ± 0.04	6.682 ± 0.08	0.050	2.5%

Fitted mean and 1σ X and Y core locations are shown compared to the true position. Integral error distributions were obtained for the radial error ($R = \sqrt{X^2 + Y^2}$) and the distances containing 50% of the data points, and the percentage of points outside 0.25 km of the true core location are presented.

Table 4
Reconstruction results for stereo, timing and stereo-timing techniques on 300, 3 EeV Monte Carlo showers performed by Elbert [13]

Fit type	Space angle error	
	Median (50%)	90% Level
Stereo	0.5°	5°
Timing	0.7°	4°
Stereo-timing amplitude weighting	0.24°	0.8°
Stereo-timing amplitude fitting	0.12°	0.6°

Reconstruction was performed assuming the HiRes detector consisted of 54 mirrors in two azimuthal rings at each of two sites, and that all timing systematics were understood (which should be the case for the FADC electronics).

that the results for the timing fit from October 12th presented in Table 1 (with opening angles generally greater than 10°) are comparable to those obtained with the Monte Carlo simulations by Elbert (see Table 4) [13]. The simulation assumed a two site detector comprised of two full azimuthal rings covering from 3°–30° in elevation. Importantly, Elbert assumed that the sites were well synchronised in time and all timing systematics were accounted for. This assumption is appropriate for the FADC electronics system to be used at HiRes-2, but is not necessarily true for the sample-and-hold systems used by the prototype detector. We believe we have been partially successful in correcting for time slewing systematic effects, with time fitting results not too different from the Monte Carlo predictions for the detector.

As was suggested by this earlier Monte Carlo work [13], stereo-timing fitting overcomes many of the small opening angle problems present in stereo fitting to provide generally more accurate reconstruction. At small opening angles, stereo fitting alone was found to systematically shift the fitted core location away from the

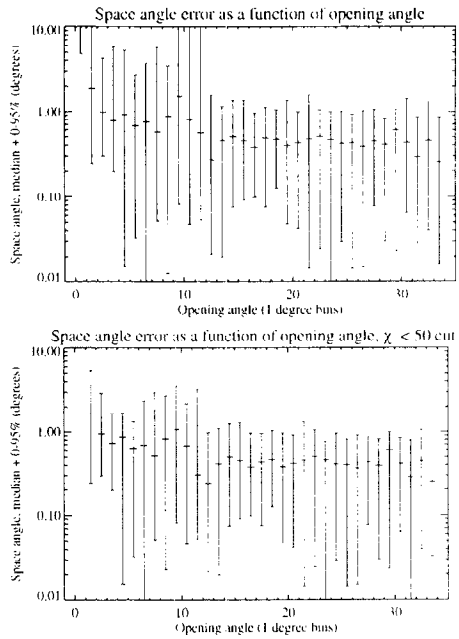

Fig. 9. Space angle error as a function of opening angle for stereo-timing fit for combined Laserscope data from 12th and 15th of October 1996. Application of a $\chi^2 < 50$ cut reduces the 95% error level so that most events are reconstructed to better than 1° (note the use of a log scale on the y-axis).

detectors (by as much as 1 km in the data from the 15th) in conjunction with increasing the zenith angle, resulting in a larger space angle error. Stereo-timing fits improve the situation because the fitter is restricted by the PMT triggering times – moving/twisting the trajectory away from the detector will have a detrimental effect on the timing χ^2 component thus preventing such behaviour.

The reconstruction accuracy, as a function of opening angle, for stereo-timing is presented in Fig. 9. These figures plot the median space angle and the 0–95% range as a function of opening angle (this range is effectively the 2σ error), before and after applying a $\chi^2 < 50$ cut. The $\chi^2 < 50$ cut was used to reject the occasional cases that failed the fitting process. After application of the $\chi^2 < 50$ cut, it can be seen that the median error is almost always less than 1°, and is generally around 0.4° for opening angles greater than 10°. The 95% error is also generally less than 1°, increasing slightly as opening angle decreases (at small opening angles the poor performance of stereo does have a limiting effect on the performance of stereo-timing fitting).

Encouragingly, these results are not significantly poorer than those obtained with the Monte Carlo simulations (Table 4) which were performed with a much more favourable opening angle range (0° to 180°) and an assumption that time slewing effects were completely compensated for. Indeed, the stereo geometries encountered in the prototype data set, with their small opening angles, are severe tests of any stereo technique. These results give us confidence that we can accurately reconstruct the arrival directions of EAS to within one degree *at least* 95% of the time.

5. Reconstruction accuracy for HiRes stage 1.0

The configuration of the Stage 1.0 HiRes detector is significantly different from that of the prototype. HiRes Stage 1.0 consists of a single ring of mirrors at HiRes-1 (3°–16.5° in elevation, 360° in azimuth) and two rings of mirrors at HiRes-2 (3°–30° in elevation, 336° in azimuth) designed to maximise the high energy aperture.

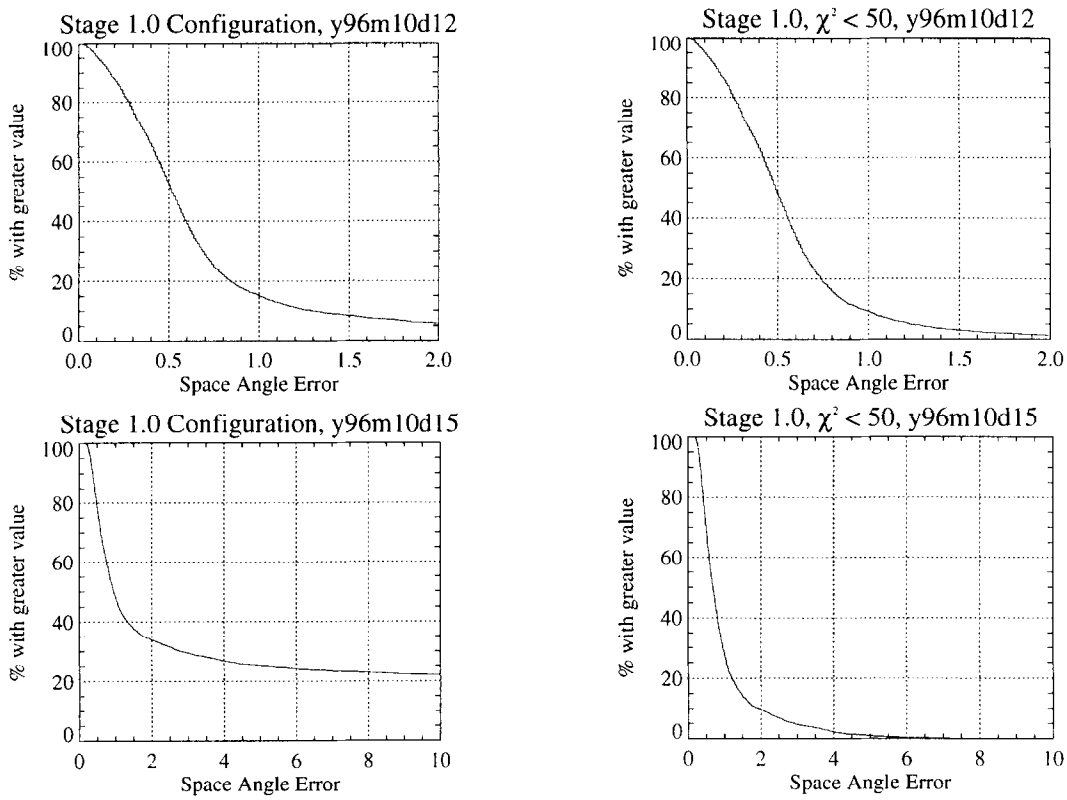

Fig. 10. Space angle error distributions using the HiRes Stage 1.0 configuration (both rings at HiRes-2 and only ring 1 mirrors at HiRes-1). Note how the tail of badly reconstructed events is eliminated by application of the $\chi^2 < 50$ cut.

Whilst the reconstruction programs were written for the reconstruction of prototype data, it is obviously of interest to examine how they might perform on data from the Stage 1.0 configuration. Such an analysis was performed on the data set already described, by rejecting all information from the top four elevation rings of HiRes-1. All information from HiRes-2 was retained. This restriction reduced the number of reconstructable events from 4343 to 2835 on the 12th, and from 6811 to 3819 on the 15th. The space angle error distributions for these events were calculated for both the Stage 1.0 configuration and the prototype configuration. The results from October 12th are summarised in Table 5 and the results from October 15th are summarised in Table 6. Space angle error distributions for Stage 1.0 results are presented in Fig. 10 (for both nights, before and after the $\chi^2 < 50$ cut).

The results are encouraging as they illustrate that fitting does very well despite the loss of 54° of zenith coverage. The majority of events were well reconstructed although there was a large number of events at small opening angles that were poorly reconstructed. These events were investigated and it was found that the majority of them occurred when the laser tracks were clipping the outside vertical edge of a mirror. Given that Stage 1.0 of the HiRes detector will consist of full azimuth rings, such gaps will not exist. This edge clipping prevents the observation of the full lateral width of the shower and, as the fitting is geometrically based (it uses the off-plane angle to estimate the PMT amplitude), it represents a loss of information. Such clipping also limits the tracklength and the number of PMTs in the event making reconstruction more difficult.

Again, the reader is reminded that the range of laser geometries represented in this data set poses a real test for any reconstruction technique. The real Stage 1.0 data set will contain many events with more favourable opening angles.

Table 5
Reconstruction results for Laserscope data from the 12th of October

Space angle error	50%	90%	% > 2°
Prototype configuration	0.45°	0.9°	2%
Stage 1.0 configuration	0.5°	1.3°	6%
After $\chi^2 < 50$ cut			
Prototype configuration	0.4°	0.8°	0.3%
Stage 1.0 configuration	0.5°	1.0°	1%

Stage 1.0 configuration consisted of using ring 1 mirrors at HiRes 1 (mirrors 5 and 7) and all four HiRes 2 mirrors. The same set of 2835 events was used to produce all the statistics.

Table 6
Reconstruction results for Laserscope data from the 15th of October

Space angle error	50%	90%	% > 2°	% > 10°
Prototype configuration	0.75°	3°	12%	3%
Stage 1.0 configuration	1.0°	57°	34%	22%
After $\chi^2 < 50$ cut				
Prototype configuration	0.75°	1.3°	2.5%	0
Stage 1.0 configuration	0.75°	2.0°	10%	0

Stage 1.0 configuration consisted of using ring 1 mirrors at HiRes 1 (mirrors 5 and 7) and all four HiRes 2 mirrors. The same set of 3819 events were used to produce all the statistics.

6. Contribution to energy and shower maximum measurements

Errors in the geometrical reconstruction will contribute to errors in the determination of cosmic ray energy and depth of shower maximum, X_{max}. However, there are other sources of uncertainty which will be as important, or more important. Measuring energy and X_{max} requires a good measurement of the shower's longitudinal development profile. Uncertainties in that profile may derive from atmospheric attenuation uncertainties related to the presence of aerosols; calibration uncertainties; statistical fluctuations in the number of received photoelectrons and the night sky background; and uncertainties in the fluorescence production efficiency. These topics are being addressed and will be discussed in forthcoming publications on energy and X_{max} measurements.

The effect of geometrical errors on these parameters can be estimated in simple ways. In the energy measurement the main geometrical effect will be to introduce an uncertainty in the attenuation of light between the shower and detector. For a distance error of Δr the fractional change in the attenuation correction will be approximately $e^{\Delta r/\lambda}$ where λ is the attenuation length of the light. Simulations of the Stage 1 aperture show that the average attenuation length at 350 nm for 10^{19} eV showers is approximately $\lambda = 13$ km, averaged over all viewing angles. Even if we take a distance uncertainty of 0.25 km (large compared with the core location errors discussed in this paper) we get a resulting attenuation correction change of only 2%. This is small compared with estimated uncertainties in the attenuation length itself (leading to energy uncertainties of order 10%), and uncertainties in calibration, also of order 10%.

In X_{max} measurements, an uncertainty in the zenith angle of the shower axis can lead to an uncertainty in the position of shower maximum. Given a photomultiplier with a direction towards X_{max}, an error in the angle of the track within the shower–detector plane will lead to an incorrect assignment of the depth viewed by the tube. Consider a simple example of a shower at a zenith angle of 45° contained within a vertical shower–detector plane (i.e. angle $\Psi = 45°$). An error of 1.0° in this angle (an extreme value from Table 5) would lead to a 15 g cm^{-2} error in X_{max} for a typical mean value of 850 g cm^{-2}. This is an extreme case with all of the space

angle error present as an error in Ψ within the shower–detector plane. It also ignores the fact that we have stereo views of the profile allowing for investigation of these effects. Simulations of Stage 1 have indicated that the expected r.m.s. X_{max} uncertainty, including contributions from geometry and photon statistics, is approximately 30 g cm^{-2} [3].

7. Conclusions

The geometrical reconstruction accuracy of the HiRes detector has been investigated using Laserscope generated events viewed in stereo. Fitting results using the HiRes prototype indicate a median space angle error of 0.4° with 95% of errors below 0.9° for shower–detector plane opening angles down to a few degrees. Results for the Stage 1.0 detector are expected to be only slightly degraded.

Geometry reconstruction errors form a component of the total error in other parameters of interest such as primary energy and X_{max}. Whilst it is a component, we have been able to show that geometrical accuracy is at a level that does not dominate these errors.

Acknowledgements

We are indebted to the staff of Dugway Proving Grounds for their continued cooperation and assistance. It is also a pleasure to acknowledge the support of the technical staff at our institutions. This work is funded in part by the National Science Foundation under grants Numbers PHY 95-12810, 93-22298, 93-21949, 92-15987 and by the Australian Research Council.

References

[1] C.R. Wilkinson, The Application of High Precision Timing in the High Resolution Fly's Eye Cosmic Ray Detector, Ph.D. Thesis (University of Adelaide, 1998).
[2] R.M. Baltrusaitis, R. Cady, G.L. Cassiday et al., Nucl. Instr. & Meth. Phys. Res. A 240 (1985) 410.
[3] University of Utah, Staged Construction Proposal for the High Resolution Fly's Eye (HiRes) Detector, NSF Proposal (1993).
[4] D.J. Bird, J. Boyer, G.F. Chen et al., Proceedings of the 24th ICRC, Rome, Vol. 3 (1995) p. 504.
[5] C.R. Wilkinson, T. Abu-Zayyad, M. Al-Seady et al., The High Resolution Fly's Eye prototype cosmic ray detector, in preparation.
[6] D.J. Bird, J. Boyer, G.F. Chen et al., Proc. 24th ICRC, Rome, Vol. 3 (1995) p. 746.
[7] J. Smith, Tokyo Workshop on Techniques for the Study of Extremely High Energy Cosmic Rays, M. Nagano, ed. (ICRR, University of Tokyo, 1993) p. 250.
[8] J. Smith, Tokyo Workshop on Techniques for the Study of Extremely High Energy Cosmic Rays, M. Nagano, ed. (ICRR, University of Tokyo, 1993) p. 265.
[9] D.J. Bird, J. Boyer, G.F. Chen et al., Proc. 24th ICRC, Rome, Vol. 3 (1995) p. 548.
[10] T. Abu-Zayyad, M. Al-Seady, K. Belov et al., Proc. 25th ICRC, Durban, Vol. 5 (1997) p. 325.
[11] T. Abu-Zayyad, M. Al-Seady, K. Belov et al., Proc. 25th ICRC, Durban, Vol. 7 (1997) p. 209.
[12] T. Abu-Zayyad, M. Al-Seady, K. Belov et al., Proc. 25th ICRC, Durban, Vol. 7 (1997) p. 213.
[13] J.W. Elbert, Tokyo Workshop on Techniques for the Study of Extremely High Energy Cosmic Rays, M. Nagano, ed. (ICRR, University of Tokyo, 1993) p. 158.
[14] W.H. Press, B.P. Flannery, S.A. Teukolsky, W.T. Vetterling, Numerical Recipes (Cambridge Univ. Press, Cambridge, 1988).
[15] T. Abu-Zayyad, M. Al-Seady,, K. Belov et al., Proc. 25th ICRC, Vol. 5 (1997) p. 349.
[16] M.J. Kidd, Properties of Extensive Air Showers around 10^{17} eV, Ph.D. Thesis (University of Illinois, 1997).